# Chromophores from photolyzed ammonia reacting with acetylene: Application to Jupiter's Great Red Spot

R. W. Carlson*, [1]. K. H. Baines[1], M. S. Anderson[1], G. Filacchione[2], A. A. Simon[3]

[1] Jet Propulsion Laboratory, California Institute of Technology, Pasadena, California, USA
[2] Istituto di Astrofisica e Planetologia Spaziali, Roma, Italy
[3] NASA Goddard Space Flight Center, Greenbelt, Maryland USA

* Corresponding Author

Mailing address:

Robert W. Carlson
Mail Stop 183-601
Jet Propulsion Laboratory
4800 Oak Grove Dr.
Pasadena, CA 91109
Phone: 818-354-2648
E-Mail: Robert.W.Carlson@jpl.nasa.gov

Manuscript pages: 20
Figures: 6
Tables: 1

Keywords: Jupiter, atmosphere; Photochemistry, Atmospheres, chemistry, Atmospheres, composition, Organic chemistry

**Abstract**

The high altitude of Jupiter's Great Red Spot (GRS) may enhance the upward flux of gaseous ammonia ($NH_3$) gas into the high troposphere, where $NH_3$ molecules can be photodissociated and initiate a chain of chemical reactions with downwelling acetylene molecules ($C_2H_2$). These reactions, experimentally studied earlier by Ferris and Ishikawa (1987; 1988), produce chromophores that absorb in the visible and ultraviolet regions. In this work we photolyzed mixtures of $NH_3$ and $C_2H_2$ using ultraviolet radiation with a wavelength of 214 nm and measured the spectral transmission of the deposited films in the visible region (400-740nm). From these transmission data we estimated the imaginary indices of refraction. Assuming that ammonia grains at the top of the GRS clouds are coated with this material, we performed layered sphere and radiative transfer calculations to predict GRS reflection spectra. Comparison of those results with observed and previously unreported *Cassini* visible spectra and with true-color images of the GRS show that the unknown GRS chromophore is spectrally consistent with the coupled $NH_3$-$C_2H_2$ photochemical products produced in our laboratory experiments. Using high-resolution mass spectroscopy and infrared spectroscopy we infer that the chromophore-containing residue is composed of aliphatic azine, azo, and diazo compounds.

## 1. Introduction

Jupiter is colored using a basic palette of white, yellows, and browns (Peek, 1958; Taylor et al., 2004) for the belts, zones, and also for many of the vortex features. However for Jupiter's largest storm, the Great Red Spot (GRS), a deep orange, almost red, pigment is additionally found. The identities of the chromophores that produce Jupiter's colors are still unknown although many suggestions have been advanced (see reviews by Sill (1975) and West et al.(1986)). The three main candidates at present, all potentially produced by ultraviolet photolysis in the jovian atmosphere, are (1) organic molecules (Sagan and Miller, 1960; Sagan et al., 1967; Woeller and Ponnamperuma, 1969; Sagan and Khare, 1971; Khare and Sagan, 1973; Ferris and Chen, 1975; Ponnamperuma, 1976; Ferris and Morimoto, 1981; Ferris and Ishikawa, 1987; Ferris and Ishikawa, 1988), (2) red phosphorous from phosphine photolysis (Prinn and Lewis, 1975; Ferris and Benson, 1981; Ferris et al., 1982; Ferris et al., 1984; Ferris and Khwaja, 1985; Guillemin et al., 1995; Guillemin et al., 1997; Guillemin et al., 2001), and possibly (3) hydrogen and ammonium polysulfides and elemental sulfur (Owen and Mason, 1969; Lewis and Prinn, 1970; Prinn, 1970) although these were suggested for lower troposphere chromophores.

A possible clue to the production of the GRS chromophore is the great height of this storm, being one of the tallest vortex features on the planet. This was illustrated using Galileo Near Infrared Mapping Spectrometer (NIMS) spectral mapping (Baines et al., 1996; Irwin et al., 1999) and Solid State Imaging (SSI) data (Simon-Miller et al., 2001a). Analysis of NIMS observations, illustrated in Fig. 1 and described in the Appendix, show that the GRS cloudtop extends about 6 km above the main ammonia ($NH_3$) cloud deck, reaching pressure levels of approximately 200 mbar.

It is often postulated that the GRS vortex upwells gas from below. At the 700-mbar level, the GRS shows an enhancement in the $NH_3$ mixing ratio (Sada et al., 1996). At higher altitudes, at the 550-mbar to 380-mbar levels, little enhancement is found relative to adjacent regions (Lara et al., 1998; Fletcher et al., 2010) although Achterberg et al. (2006) suggest a measurable increase at 438 mbar. Above the 300 mbar level a relative depletion is found for the GRS (Tokunaga et al., 1980; Griffith et al., 1992; Edgington et al., 1999) as well as a much steeper gradient (Tokunaga et al., 1980; Irwin et al., 2004), consistent with upward flow of gaseous $NH_3$ and loss by photodissociation and condensation.

At the high altitudes of the GRS, solar ultraviolet radiation with wavelengths > ~200 nm can penetrates and dissociate $NH_3$ molecules as $NH_3 + h\nu \rightarrow NH_2 + H$ (Prinn, 1970; Visconti, 1981; Cheng et al., 2006). The altitude (pressure) for maximum absorption rate is approximately 200-250 mbar for a solar zenith angle of zero and increases for non-normal illumination. In this altitude range acetylene, produced higher up by shorter wavelength solar ultraviolet-initiated photochemistry, diffuses down and is destroyed by reactions with amino radicals ($NH_2$) and atomic hydrogen and by other photochemical processes (Kaye and Strobel, 1983; Moses et al., 2010).

Mixtures of gaseous acetylene and ammonia are known to react under $NH_3$ photolysis and produce - in addition to HCN – a condensate that absorbs radiation in the ultraviolet and visible region (Ferris and Ishikawa, 1987; Ferris and Ishikawa, 1988), however measurements of the spectral absorption properties of this potential chromophore are not available (see summary of prior related work in Section 2, below). Furthermore, there are few spectra of the GRS in the literature. In this work we extend the ammonia – acetylene photolysis experiments (Section 3) and obtain the imaginary index of refraction of the colored condensate. Employing electromagnetic scattering theory for layered spheres and radiative transfer calculations we simulate reflection spectra of the GRS (Section 4). We then compare our laboratory results to newly analyzed *Cassini* visible spectra, *Hubble Space Telescope* (HST) data, and ground-based measurements. We discuss the composition of the chromophore-containing residue using mass and infrared spectroscopic measurements work and suggest potential observational tests (section 5). Jovian photochemical flux considerations and possible relations to other red features in Jupiter's atmosphere are briefly discussed in Section 6.

## 2. Prior Studies of Ammonia-Acetylene Gases and related Reactions

### Ammonia + Methane

The early jovian chemical simulations used electrical discharges and are of interest here because acetylene is produced and the ultimate reaction products may be similar to the present experiments. Sagan and Miller (1960) electrically sparked a methane, ammonia, and hydrogen gas mixture and produced ethane ($C_2H_6$), ethylene ($C_2H_4$), acetylene ($C_2H_2$), hydrogen cyanide (HCN), and acetonitrile ($CH_3CN$).

In a series of experiments by Ponnamperuma and colleagues, the products produced by electrical discharges in ammonia and methane gases were studied, first finding production of HCN, nitriles, and reddish-brown solid residues (Woeller and Ponnamperuma, 1969). Acid hydrolysis of the residues gave amino and imino acids (Chadra et al., 1971) and Molton and Ponnamperuma (1974) performed mass spectroscopic studies of the condensed products, with their results suggesting the formation of aminonitriles.

Ferris and coworkers (Ferris and Chen, 1975; Ferris and Morimoto, 1981; Ferris et al., 1982) studied the photolysis of $NH_3$ in the presence of $CH_4$ wherein the hot hydrogen atoms liberated by 185-nm photons possessed sufficient kinetic energy to overcome the 0.6 eV reaction barrier of $CH_4$, producing the methyl radical. Subsequent reactions yielded $C_2$-and $C_3$-hydrocarbons, methylamine ($CH_3NH_2$) and hydrogen cyanide (HCN), as well as $H_2$, $N_2$ and hydrazine ($N_2H_4$). This mechanism for chemical destruction of $CH_4$ is unlikely to be prevalent on Jupiter due to thermalization of the energetic H atoms by the dominant $H_2$ gas (Ferris and Morimoto, 1981; Ferris et al., 1982).

Ammonia + Acetylene

Kaye and Strobel (1983) first suggested that HCN is formed in Jupiter's atmosphere from photolyzed $NH_3$ reacting with acetylene and Moses et al. (2010) recently performed a comprehensive model of Jupiter's coupled $NH_3$ - $C_2H_2$ photochemistry. The initial production of molecules containing carbon and nitrogen can occur in several path ways, beginning when ammonia is photodissociated into $NH_2$ + H. The amino radical ($NH_2$) can react with $C_2H_2$ in a three-body reaction. Additionally, the liberated hydrogen atoms react with $C_2H_2$ and its reaction products, forming $C_2H_3$ and other radicals, which react with $NH_2$ to form N-containing hydrocarbons.

An early study by Tsukada et al. (1972) indicated that the heterocyclic molecule pyrrole ($C_4H_4NH$) was formed in $NH_3$-$C_2H_2$ photolysis. Comprehensive investigations of the photochemistry of $NH_3$ + $C_2H_2$ were performed by Ferris and Ishikawa (1987; 1988), who demonstrated HCN production and suggested that this molecule is formed from the intermediate products acetaldazine ($CH_3CH{=}N{-}N{=}CHCH_3$) and subsequent acetonitrile ($CH_3CN$). An ultraviolet absorbing brownish residue formed with infrared spectral characteristics dissimilar to acetylene polymers, but instead showed CH stretch bands of the methyl and methylene functional groups, indicating the presence of saturated

aliphatic hydrocarbons. The presence of –NH and $-NH_2$ groups was indicated by the NH stretch feature at 3300 $cm^{-1}$.

The coupled photochemistry of $NH_3$ and $C_2H_2$ was further studied and numerous intermediate and final reaction products (e. g., azines, imines, amines, nitriles, and others) and their quantum yields determined Keane (1995) . This work enabled predictions to be made for the Galileo entry probe mass spectrometer measurements (Keane et al., 1996) and formed the experimental basis for a comprehensive model of jovian ammonia-acetylene photochemistry (Moses et al., 2010).

## 3. Photolysis Measurements

Our experiments were similar to those performed by Ferris and Ishikawa (1987; 1988), using ammonia and acetylene in different proportions but we also added methane in some experiments. The experiments were performed at ambient temperatures. A cartoon illustrating the experimental apparatus and their arrangement is shown in Fig. 2.

The $NH_3$ and $C_2H_2$ gases were both from Matheson with purities of 99.999% and 99.6%, respectively. The $C_2H_2$ sample, as delivered, was dissolved in acetone ($CH_3COCH_3$) but was further purified by repeated vacuum distillation, with the acetone content measured by mass spectroscopy using a quadrupole residual gas analyzer (RGA). Typical acetone levels achieved were < 0.1% mole fraction relative to $C_2H_2$. The methane gas was from Airgas and of ultrahigh purity grade (99.99%). The gases were mixed in a 300-ml stainless steel high-vacuum manifold and connected to the photolysis cell with a Viton O-ring seal with a low-vapor pressure ($5 \times 10^{-13}$ Torr) tetrafluorethylene grease. The system was operated as a closed system except for occasional gas sampling for infrared and mass spectra monitoring. The large manifold volume relative to the volume of the photolysis cell enabled us to generate measurable amounts of photolysis products, limited only by its ultraviolet absorption.

We used a Zn lamp (UV Products) that emits ultraviolet (UV) radiation in three lines at wavelengths $\lambda$ = 202.5, 206.2, and 213.9 nm with measured relative intensities of 1, 2, and 100 respectively. The UV energy flux incident on the cell window was about 10 mW or $10^{16}$ 214-nm photons $s^{-1}$. Photolysis at this flux rate occurs at the beginning of the irradiation but the rate decreased rapidly as the ultraviolet- and visible-absorbing film

formed. Although $C_2H_2$ can be photodissociated in this near-threshold region (Mordaunt et al., 1998), the absorption cross sections (Nakayama and Watanabe, 1964) are small compared with those of ammonia (Chen et al., 1999) and we estimate that less than 1/500 of the UV photons are absorbed by $C_2H_2$ in the mixtures used here. The photolysis cells were 25- and 50-mm long, 19-mm inside diameter glass cells with UV-grade quartz windows. No spectral differences were found for films made with different length cells. Similar films were also made using a Teflon cell with $CaF_2$ windows.

We periodically measured the spectral transmission of the films as they developed with time. Prior to the start of the irradiations the photolysis cell was placed in the optical path between a tungsten-halogen incandescent source and a grating spectrometer. Radiation from this lamp was collimated with a $CaF_2$ lens, passed through the cell and an optical filter transmitting radiation for $\lambda > 400$ nm, and then focused with a second $CaF_2$ lens to image the lamp's filament on the spectrometer's entrance slit. The spectrometer was an Acton 0.5-m Czerny-Turner mount with a 1200 lines/mm grating. Reference spectra in the 400 to 740-nm interval with a resolution of 4 nm were obtained of the evacuated cell. The cell was then filled with a mixture of $C_2H_2$ and $NH_3$ gas, and, in some cases, $CH_4$. Guided by the work of Ferris and Ishikawa (1987; 1988), the initial $NH_3$ to $C_2H_2$ molar ratio was generally ~ 10:1 with an $NH_3 + C_2H_2$ pressure of ~ 120 Torr (158 mbar), although some experiments were performed at a lower molar ratio and total pressures (Table 1). A 10:1 molar ratio of $NH_3$ to $C_2H_2$ occurs at approximately the 130 mbar level in the jovian atmospheric model of Moses et al. (2010) and is within the 100 – 160 mbar region where most of the initial production of the carbon- nitrogen molecules occurs (see the supplementary information of Moses et al., 2010). The partial pressures are orders of magnitude higher in the laboratory measurements compared to $NH_3$ and $C_2H_2$ in Jupiter's upper troposphere, but the total pressure is comparable so 3-body reactions would be expected to occur at approximately the same rates. When $CH_4$ was added its partial pressure was about twice greater than that of $NH_3$. Spectra of the filled but un-irradiated cell were then obtained, and showed no change from the empty-cell spectra, as expected. The UV lamp was then positioned and irradiation begun. At intervals that increased with time the photolysis lamp removed and transmission spectra were obtained.

Table 1. Summary of major experiments

| No. | System | Molar ratios | Total pressure, Torr | Notes |
|---|---|---|---|---|
| 1 | $NH_3 + C_2H_2$ | 10:1 | 124 | UV-Vis absorption |
| 2 | $NH_3 + C_2H_2$ | 5:1 | 130 | " " " |
| 3 | $NH_3 + C_2H_2$ | 10:1 | 93 | " " " |
| 4 | $NH_3 + CH_4$ | 1:2 | 118 | No apparent reaction |
| 5 | $NH_3 + C_2H_2 + CH_4$ | 10:1:20 | 122 | Similar to $NH_3 + C_2H_2$ cases |
| 6 | $NH_3 + C_2H_2$ | 12:1 | 15 | With $SiO_2$ powder |

During irradiation an absorbing film developed on the inner surface of the irradiated window. The growth rate of the film and its transmission diminished with time as the film's thickness and corresponding UV opacity increased. At the same time, mass spectrometer measurements showed that the acetylene fraction, relative to ammonia, decreased although the total manifold pressure remained about the same, presumably from the generation of $N_2$, $H_2$, HCN, and other products, consistent with mass spectra and infrared spectra of a condensed sample of the manifold gas (Section 5).

The films showed evidence for interference fringes (channel fringes) with amplitude modulations of approximately $\pm$ 4% and a period of ~ 5000 $cm^{-1}$ indicating films of ~ 1 μm in optical thicknesses or ~ 0.7 μm in physical thickness using a refractive index of $n$ = 1.4 (a typical value for aliphatic hydrocarbons). In order to minimize this modulation effect on the spectra we performed an average of three successive spectra, using the changing phase to form an average with muted oscillations (see Fig. 3A). Even with this averaging, it is difficult to accurately estimate the wavelength-independent extinction coefficient, which could also contain a scattering component. In general the spectra show less modulation but some still show the effect (e. g., for the 15-, 108-, and 197-hour average irradiation times). Nevertheless, the trend and spectral shape are indicated and typical of all of our $NH_3 + C_2H_2$ experiments.

Transmission spectra taken at the end of the irradiation were followed by evacuation of gas from of the cell and another transmission spectrum was obtained. No change was observed from the preceding spectrum, showing that the film material was non-volatile. A spectrum taken after air exposure similarly showed no change, indicating chemical

stability. A comparison of the lamp spectra without the cell in the path showed no change in the spectral shape to within 3%.

Addition of methane to $NH_3$ + $C_2H_2$ (Experiment No. 5) still produced a film with the same color and transmission properties. The growth rate was little affected by added $CH_4$. An experiment with no acetylene but only $NH_3$ and $CH_4$ did not produce any measurable absorption, as expected owing to the $CH_4$ reaction barrier.

The films that are produced are yellow in reflection and pale orange in transmission. They are limited in thickness by their absorbance in the photolyzing ultraviolet region. As the films grew, the amount of transmitted ultraviolet radiation and the resulting growth rate diminished rapidly. In order to produce more opaque films, we placed a millimeter-thick layer of silica powder, consisting of 10-μm diameter spheres (AngstromSphere), into an absorption cell and introduced a sample of $NH_3$ + $C_2H_2$ gas (Experiment No. 6 in Table 1). Lower partial pressures were used to ensure penetration of photons well into the gas + powder medium to coat the spheres with the chromophore. The cell was irradiated from below for 6 days with the cell occasionally shaken to redistribute the powder and to provide fresh grain surfaces near the bottom window for collection of the generated photoproducts. After irradiation, a photograph (Fig. 4A) of the transmitted light was obtained using a white light emitting diode (LED) lamp with a color temperature somewhat greater than that of the sun. A colored pigment was found and is compared to GRS colors on the following Section.

## 4. Great Red Spot Spectral and Color Comparison

There are surprisingly few spectra of the GRS to compare with laboratory measurements. Here we use observations by *Cassini's* VIMS-V (visible) channel, an imaging spectrometer that covers the 300 – 1050 nm region at a spectral resolution of 1.46 nm and an angular resolution of 167 μrad $\times$ 167 μrad per pixel (Miller et al., 1996; Brown et al., 2004; Coradini et al., 2004 ). These spatially resolved spectra (Fig. 3B) of the GRS were obtained during *Cassini's* December, 2000 flyby of Jupiter, acquired at 2000-339 08:31:01.684 with an integration time of 1.28 sec and denoted Cube C23 V1354610545. The raw data cubes are available on NASA's Planetary Data System along with calibration routines. The ground calibration is described by Capaccioni et al. (1998) and Filacchione (2006). The GRS was observed at a phase angle of 9.7° and within 10-15° of local noon, similar to observations obtained from Earth. The spacecraft range to

Jupiter for this observation was 26.4 $\times$ $10^6$ km, projecting a pixel footprint of ~ 4,400 km $\times$ 4,400 km on Jupiter, smaller than the nominal 10,000 km $\times$ 25,000 km GRS. We show two spectra from this observation, the first being for the central pixel and the second being the average of the central and adjacent eastern and western pixels. There is a second GRS observation by *Cassini* (V1356904960), obtained with better spatial resolution but at a high phase angle and not geometrically comparable to ground-based and HST observations. Data from the IR portion of *Cassini* VIMS were also obtained during both observations and discussed briefly in Section 5.

Fig. 3B also contains the measurements performed by Orton (1975) using a scanner at fixed wavelengths, HST imagery data in several filters (Simon-Miller et al., 2001b; Pérez-Hoyos et al., 2009; Strycker et al., 2011; Simon et al., 2015), and albedo values for the HST image shown in Fig. 4B and discussed below.

To compare our laboratory results with observations we calculated the reflectance, assuming the cloud-top ammonia particles are coated with a thin layer of chromophore, although other colored aerosol formation and mixing scenarios are possible but not investigated here. The grains are assumed spherical with a log-normal distribution of radii and an average diameter of 1 $\mu$m. Optical constants for the chromophore were found using the 70-hour transmission data (Fig. 3A) with the thickness and assumed value of real index noted earlier. Data from Martonchik et al. (1984) for were used for the $NH_3$ optical constants. Mie calculations for layered spheres (Toon and Ackerman, 1981) were performed for layer thicknesses of $\delta R/R$ = 1/100, 2/100, 4/100. 6/100, and 16/100. Using the calculated single scattering albedos and asymmetry parameters, we employing similarity relations (Van De Hulst, 1980; Hapke, 1993) to find the equivalent single scattering albedo for isotropic scattering and the reflectance for a semi-infinite cloud using the formulation of Hapke (1993). Rayleigh scattering and extinction were included. In order to compare these results with observations performed at different times and different GRS colors, we normalized the observations and computed spectra to a value of 0.83 at 673 nm, approximating typical I/F values for Jupiter at that wavelength ($I$ is the observed radiance and $\pi F$ is the solar irradiance). The results are shown in Fig. 3B. The computed spectra, although approximate, mimic the general trend indicated by the ground and HST-derived data and the *Cassini* spectra.

A color comparison is shown on Fig. 4, where we have used a HST images obtained in June 2008 (Program GO11498) and compare a true color image to a photograph of the

coated silica particles of Experiment No. 6. The HST color image in Fig. 4B uses absolute I/F values at red (673 nm), green (502 nm), and blue (410 nm) wavelengths without contrast enhancement to render an image that most closely resembles the color of the GRS at that time. Images were obtained at 255, 343, 375, 390, 410, 437, 469, 503, 673, and 889 nm with exposure times of 230, 140, 100, 35, 8, 14, 10, 8, 4, and 40 seconds, respectively. Comparison of these two images shows similar colors, and a spectral comparison of the filter data obtained in the HST observation with modelled spectra (Fig. 3B) indicates spectral similarities.

**5. Chromophore composition and possible HCN**

The laboratory transmission spectra do not exhibit spectral characteristics that provide any chemical identification, so here we investigate the chemical composition of the experimental chromophore-containing residue using two techniques, mass spectroscopy and infrared spectroscopy. Mass spectroscopy can tell us which atoms are present and their number, while infrared spectroscopy indicates the functional groups that are present. Unique identification of the molecules present in the residue is not possible with just this information but the classes of molecules can be suggested.

The mass spectroscopic measurements used open-air ionization produced by Penning ionization using metastable helium (He $2^3S$). This is coupled to a time-of-flight (TOF) mass spectrometer, forming a system termed DART (Direct Analyis in Real Time, Cody et al., 2005). This soft ionization enables molecules that are otherwise difficult to ionize and volatilize to be readily introduced into the mass spectrometer system. The ions that are produced in ambient conditions are protonated parent molecules $MH^+$, where M is the parent molecule and the proton arises from atmospheric water vapor. The TOF spectrometer has a very wide mass range and individual masses can be measured with accuracy better than 5 mDa. This enables molecular identification of specific mass peaks using the variations in atomic mass among the elements and their isotopes (see below). The residue was extracted with dichloromethane ($CH_2Cl_2$), the solvent was allowed to evaporate, and the residue then exposed to the beam of excited He of the DART system, forming the mass spectrum shown in Fig 5. A mass calibration run using polyethylene glycol standards (PEG 600) was also performed. No oxygen-containing compounds were found, indicating no contamination from acetone or atmospheric oxygen.

A diffuse reflectance infrared spectrum of the residue in KBr was also obtained (Fig. 6) along with a blank sample. No spectral features of dichloremethane were found nor were any features attributable to acetone or oxygen related products. The results of the DART and DRIFT analyses are discussed together below.

Referring to the DART spectrum (Fig. 5), the major mass peaks form repeating groups of three members with each member differing by 2 hydrogen atoms. The different number of H atoms indicates different numbers of singly and multiply bonded C atoms and differences in the molecules' functional groups. The group repeat interval corresponds to two methylene groups, $-CH_2-CH_2-$ , probably derived from $C_2H_2$ and the $C_2H_3$, $C_2H_4$, and $C_2H_5$ radicals from $C_2H_2$ + H reactions (Moses et al., 2010). The number of repeats is > 6, four of which are shown in this spectrum and at least two more at higher mass but of lesser intensity.

The high resolving power of the DART system enables us to resolve isotopic mass differences and assign the numbers of C, H, and N atoms in the molecules for each molecular mass position. $^{14}N$ and $^{12}CH_2$ have a mass difference of 13 mDa so one can distinguish nitrogen-containing compounds from hydrocarbons and determine how many N atoms are in the molecule. We determined the positions of the stronger peaks between 113 Da and 170 Da and compared the observed positions with those predicted for hydrocarbons containing 0, 1, 2, 3, or 4 nitrogen atoms,. The corresponding mean differences between the observed and predicted positions for these cases were found to be -26.1, -13.5, -1.0, 11.6, and 24.2 Da, respectively, each with a standard deviation of 0.65 Da. Only positions for the two nitrogen atom case agree with the observed positions. Therefore these data uniquely identify the relative number C. H, and N atoms in each of the three members of a group, indicated with the molecular formulas: $C_{2n}H_{4n-2}N_2$, $C_{2n}H_{4n}N_2$, and $C_{2n}H_{4n+2}N_2$. The presence of two N atoms in these molecules may be related to the azine compounds (RR'=N-N=R''R''', where R represents hydrocarbon radicals) found by Ferris and Ishikawa (1987; 1988) and Keane (1995).

The smaller peaks that are offset by +1 Da correspond to carbon and nitrogen isotopes. One can also investigate the presence of potential impurity atoms by their masses. In particular the presence of oxygen atoms was investigated and no indication of its presence was found.

In order to characterize these molecules and their functional groups we employ the infrared spectra of the photolysis product shown in Fig. 6. We first note a broad band centered at 3200 $cm^{-1}$ where the N–H stretch band is found. For amines ($–NH_2$), there are generally two peaks (the symmetric and asymmetric stretch transition, (Socrates, 2001)) so the appearance of a single band indicates the presence of mainly imine groups (=N–H). At lower frequencies ( ~ 2960-2840 $cm^{-1}$) , the methyl ($–CH_3$) and methylene ($–CH_2–$) groups indicate the presence of aliphatic hydrocarbons, mainly saturated alkanes. The peak at 2056 $cm^{-1}$ may be due to a diazo compound (>C=N=N, Socrates, 2001)) and related to the di-nitrogen compounds found by Ferris and Ishikawa and Keane. The C=N stretching band of azines (>C=N-N=C<) is indicated in the 1650-1690 $cm^{-1}$ region and the C-N band of possible azo compounds (R-N=N-R') appears at 1020 $cm^{-1}$.

The central member of the three members in each DART group is generally the most abundant and we suggest its molecular formula $C_{2n}H_{4n}N_2$ to indicate alkanes with azine and/or diazo groups, possibly also including alkene-azo compounds. The $C_{2n}H_{4n+2}N_2$ members are possibly alkanes with an azo group. The $C_{2n}H_{4n-2}N_2$ members may be unsaturated alkene-azine and alkene-diazo hydrocarbons. The complex that produces the chromophore activity is unknown, but some azo compounds are known to produce dyes.

We briefly investigated the production of HCN by freezing out at 70 K a sample of the irradiated gas and obtaining an infrared spectrum of the sample. A spectral feature was found at 2118 $cm^{-1}$ that is close to the condensed HCN position (~ 2100 $cm^{-1}$) but its definitive identification must be obtained using a gas phase spectrum. If this feature is shown to be from HCN, then its possible presence over the GRS and elsewhere may indicate enhanced coupling of ammonia and acetylene chemistry at high altitudes.

The 2056 $cm^{-1}$ feature, suggested here to be from a diazo compound, would be present in the GRS infrared spectra if $NH_3$-$C_2H_2$ photolysis produces this chromophore. We examined NIMS and *Cassini* infrared spectra for such a feature. However, there are strong and ubiquitous atmospheric gas absorption bands present that preclude any chromophore identification at NIMS and VIMS spectral resolution.

**6. Summary and Discussion**

The production of a chromophore that provides the orange-red color to the Great Red Spot may be initiated by photolysis of ammonia in the high tropospheric altitudes. The photoproducts $NH_2$ and H then react with downwelling acetylene and initiate a chemical chain, producing a solid residue that can provide color. If this is indeed the source of the GRS color, the pigments may consist of aliphatic azo, diazo, or azine compounds.

Moses et al.'s (2010) study of $C_2H_2$ and $NH_3$ photochemistry in Jupiter's atmosphere indicates that the coupling is weak due to the low eddy diffusion at the tropopause, resulting in low $C_2H_2$ flux into the troposphere and consequently low chromophore production. However, only a single eddy diffusion coefficient profile was used their work, but there could be spatial variations with latitude and the underlying meteorological conditions. Edgington et al. (1999) found that the eddy mixing rate at 250 mb is greater in the GRS region compared to regions to the north and south. Similar latitudinal variations were found in the same altitude region by Lara et al. (1998). It is plausible that GRS vortex activity could influence the dynamical properties of the atmosphere above, perhaps by the generation of upwardly propagating gravity waves. The strength of such effects could vary with time and cause the observed temporal variations in the GRS color.

Our experiments used gaseous $NH_3$ and $C_2H_2$, and we have not considered the potential photochemical role of ice and aerosols. $NH_2$ and H can be photoemitted from ammonia ice grains and chemical reactions can take place on downwelled polyacetylene aerosols. Such effects may be important and need quantification.

We note that other regions of Jupiter can be red, and in some cases, redder than the GRS as shown by Simon-Miller et al. (2013) for the North Equatorial Belt and an unusual red vortex. These features occur at lower elevations than the GRS and their spectra are different from GRS spectra, suggesting that a different chromophore may be present. However, it is also possible that the same chromophores are present but local conditions modify their optical properties.

**Acknowledgements**

RWC and KHB gratefully acknowledge funding from NASA's Planetary Atmospheres Program. Portions of this work were performed at the Jet Propulsion Laboratory, California Institute of Technology, under contract with the National Space and Aeronautics Administration. Some results were based on observations made with the

NASA/ESA *Cassini* spacecraft and the *Hubble Space Telescope*. Data from the latter were obtained from the Data Archive at the Space Telescope Science Institute, operated by the Association of Universities for Research in Astronomy, Inc., under NASA Contract NAS 5-26555. These observations are associated with program GO11498.

## APPENDIX

Figure 1 shows the cloudtop altitude structure of the Great Red Spot (GRS) as derived from a spectral mapping mosaic acquired by the Near-Infrared Mapping Spectrometer (NIMS) onboard the Galileo Orbiter on June 26, 1996 during the Galileo spacecraft's first orbit. As described by Baines et al. (2002) , the mosaic of the Great Red Spot and its environs were acquired in 23 discrete colors from 0.74 to 5.21 μm with an average spatial resolution of 730 km/pixel given the average spacecraft distance of 1.46 $10^6$ km and the NIMS pixel field of view of 500 μrad $\times$ 500 μrad This resolution – comparable to that acquired from Earth with 0.25-arcsec seeing near jovian opposition – allows a detailed study of Jupiter's spatial and vertical structure.

To determine the cloudtop altitude, we utilize the well-established radiative transfer algorithms for inhomogeneous atmospheres used previously in preliminary analyses of the Great Red Spot (Baines et al., 1996; Irwin et al., 1999) and, more recently, of other jovian features (Baines et al., 2013). For each point in the GRS mosaic, the cloudtop altitude is derived from a combined analysis of the apparent albedo I/F observed at three wavelengths: (1) the pseudo-continuum wavelength at 1.89 μm, and (2) strong gas absorptions by methane and hydrogen at 1.76 and 2.12 μm, respectively. In this model, the cloud opacity is assumed to be distributed uniformly with pressure (i.e., unity for the ratio of particle scale height to that of the atmospheric gas), the cloud bottom is assumed to be the $NH_3$ condensation level at 0.7 bar, and the double Henyey-Greenstein phase function of Tomasko et al. (1978) is assumed for the particles. Below the GRS, underneath an aerosol-free layer extending downward from the 0.7-bar cloud bottom, an optically thick ($\tau_C >> 1$) lower cloud is assumed placed deep in the atmosphere. Its pressure is found to be nominally near 2.8 bar as determined from 1.6-μm pseudo-continuum observations assuming the single-scattering albedo found at 1.89-μm, detailed below. We note that, given that our cloudtop-determining wavelengths are strongly gas-absorbing, the characteristics of the atmosphere below the upper cloud have a only minor effect on the determination of the cloudtop pressure. The zero-altitude pressure value in Fig. 1 is 1 bar and the top of the altitude scale corresponds to about 170 mbar.

In our analysis, we first determine the single-scattering albedo ($\varpi$) at 1.89 μm for a large range of cloud opacities ($\tau_{Cl}$) and cloudtop altitudes ($P_{Ct}$). We then use these 1.89-μm $\varpi$ solutions to model 1.76- and 2.12-μm I/Fs over the same range of ($\tau_{Cl}$ , $P_{Ct}$ ). For $H_2$, we use the $H_2$ pressure-induced absorption formalisms of Borysow (1992) and Birnbaun et al. (1996) for an assumed equilibrium ortho-para $H_2$ distribution, and the temperature/pressure structure of Lindal et al. (1981). To calculate the methane gas absorption, we use the exponential-sum/correlated-k (Goody et al., 1989; Lacis and Oinas, 1991) with the relevant low-temperature near-IR methane absorption coefficients of Irwin et al. (1996), and assume a methane mixing ratio of 0.0018 as determined by the Galileo Probe Mass Spectrometer experiment (Niemann et al., 1998). The adopted helium abundance is 13.6% (Niemann et al., 1998; von Zahn et al., 1998). Due to the different behavior in absorption as a function of pressure between the 2.12-μm $H_2$ absorption and the 1.76-μm $CH_4$ absorption – the former, being a pressure-induced absorption, varies its strength as the square of the pressure while the latter varies its strength linearly – we find tight solutions (uncertainties less than ≈ 10 mbar) for the cloudtop pressures that fit the I/F's at 1.76 and 2.12 μm, including their I/F uncertainties.

**References**


Achterberg, R. K., Conrath, B. J., Gierasch, P. J., 2006. Cassini CIRS retrievals of ammonia in Jupiter's upper troposphere. Icarus. 182**,** 169-180.

Baines, K. H., Carlson, R. W., Kamp, L. W., 2002. Fresh ammonia ice clouds in Jupiter - I. Spectroscopic identification, spatial distribution, and dynamical implications. Icarus. 159**,** 74-94.

Baines, K. H., Carlson, R. W., Orton, G. S., 1996. The vertical and dynamical structure of the Great Red Spot as determined by Galileo/NIMS. Bull. Amer.Astron.Soc., Vol. 28, pp. 1136.

Baines, K. H., et al., 2013. The temporal evolution of the July 2009 Jupiter impact cloud. Planetary and Space Science. 77**,** 25-39.

Birnbaum, G., Borysow, A., Orton, G. S., 1996. Collision-induced absorption of $H_2$-$H_2$ and $H_2$-He in the rotational and fundamental bands for planetary applications. Icarus. 123**,** 4-22.

Borysow, A., 1992. New model of collision-induced infrared absorption spectra of $H_2$-He pairs in the 2-2.5 micron range at temperatures from 20 to 300 K - an update. Icarus. 96**,** 169-175.

Brown, R. H., et al., 2004. The Cassini visual and infrared mapping spectrometer (VIMS) investigation. Space Science Reviews. 115**,** 111-168.

Capaccioni, F., Coradini, A., Cerroni, P., Amici, S., 1998. Imaging spectroscopy of Saturn and its satellites : vims-v onboard Cassini. Planet. Space Sci. 46**,** 1263-1276.

546 Chadra, M. S., Flores, J. J., Lawless, J. G., Ponnamperuma, C., 1971. Organic synthesis
547 in a simulated jovian atmosphere - II. Icarus. 15**,** 39-44.
548 Chen, F. Z., Judge, D. L., Wu, C. Y. R., Caldwell, J., 1999. Low and room temperature
549 photoabsorption cross sections of NH3 in the UV region. Planet. Space Sci. 47**,**
550 261-266.
551 Cheng, B.-M., et al., 2006. Absorption cross sections of $NH_3$, $NH_2D$, $NHD_2$, and $ND_3$ in
552 the spectral range 140-220 nm and implications for planetary isotopic
553 fractionation. Astrophy. J. 647**,** 1535-1542.
554 Cody, R. B., Laramee, J. A., Durst, H. H., 2005. Versatile new ion source for the analysis
555 of materials in open air under ambient conditions. Anal. Chem. 77**,** 2297-2302.
556 Coradini, A., et al., 2004 CASSINI/VIMS-V at Jupiter: Radiometric calibration test and
557 data results. Planet. Space Sci. 52**,** 661–670.
558 Edgington, S. G., et al., 1999. Ammonia and eddy mixing variations in the upper
559 troposphere of Jupiter from HST Faint Object Spectrograph observations. Icarus.
560 142**,** 342-356.
561 Ferris, J. P., Benson, R., 1981. An investigation of the mechanism of phosphine
562 photolysis. J. Am. Chem. Soc. 103**,** 1922-1927.
563 Ferris, J. P., Bossard, A., Khwaja, H., 1984. Mechanism of phosphine photolysis.
564 Application to jovian photochemistry. J. Am. Chem. Soc. 106**,** 318-324.
565 Ferris, J. P., Chen, C. T., 1975. Photosynthesis of organic compounds in the atmosphere
566 of Jupiter. Nature. 258**,** 587-588.
567 Ferris, J. P., Ishikawa, Y., 1987. HCN and chromophore formation on Jupiter. Nature.
568 326**,** 777.
569 Ferris, J. P., Ishikawa, Y., 1988. Formation of HCN and acetylene oligomers by
570 photolysis of ammonia in the presence of acetylene - Applications to the
571 atmospheric chemistry of Jupiter. J. Amer. Chem.Soc. 110**,** 4306-4312.
572 Ferris, J. P., Khwaja, H., 1985. Laboratory simulations of $PH_3$ photolysis in the
573 atmospheres of Jupiter and Saturn. Icarus. 62**,** 415-424.
574 Ferris, J. P., Morimoto, J. Y., 1981. Irradiation of $NH_3$-$CH_4$ mixtures as a model of
575 photochemical processes in the Jovian planets and Titan. Icarus. 48**,** 118-126.
576 Ferris, J. P., Morimoto, J. Y., Benson, R., Bossard, A., 1982. Photochemistry of $NH_3$,
577 $CH_4$, and $PH_3$. Possible applications to the jovian planets. Origins of Life. 12**,**
578 261-265.
579 Filacchione, G., 2006. Calibrazioni a terra e prestazioni in volo di spettrometri ad
580 immagine nel visibile e nel vicino infrarosso per l'esplorazione planetaria. Vol.
581 PhD. Universit`a Federico II, Napoli, Italy.
582 Fletcher, L. N., et al., 2010. Thermal structure and composition of Jupiter's Great Red
583 Spot from high-resolution thermal imaging. Icarus. 208**,** 306-328.
584 Goody, R., West, R. A., Chen, L., Crisp, D., 1989. The correlated-k method for radiation
585 calculations in nonhomogeneous atmospheres. J. Quant. Spect. Radiative Trans.
586 42**,** 539-550.
587 Griffith, C. A., Bezard, B., Owen, T., Gautier, D., 1992. The tropospheric abundances of
588 $NH_3$ and $PH_3$ in Jupiter's Great Red Spot, from *Voyager IRIS* observations. Icarus.
589 98**,** 82-93.
590 Guillemin, J. C., El Chaouch, S., Bouayad, A., Janati, T., 2001 Partial pressures and
591 nature of products. Application to the photolysis of $PH_3$ and $NH_3$ in the

592 atmosphere of Jupiter and Saturn. Space Life Sciences: Life in the Solar System:
593 Prebiotic Chemistry, Chirality and Space Biology, pp. 245-253.
594 Guillemin, J. C., Janati, T., Lassalle, L., 1995. Photolysis of phosphine in the presence of
595 acetylene and propyne, Gas-mixtures of planetary interest. Adv. Space Res. 16**,**
596 85-92.
597 Guillemin, J. C., LeSerre, S., Lassalle, L., 1997 Regioselectivity of the photochemical
598 addition of phosphine to unsaturated hydrocarbons in the atmospheres of Jupiter
599 and Saturn. Life Sciences: Complex Organics in Space, pp. 1093-1102.
600 Hapke, B., 1993. Theory of reflectance and emittance spectroscopy. Cambridge
601 University Press, Cambridge.
602 Irwin, P. G. J., Calcutt, S. B., Taylor, F. W., Weir, A. L., 1996. Calculated k distribution
603 coefficients for hydrogen- and self-broadened methane in the range 2000-9500
604 cm-1 from exponential sum fitting to band-modelled spectra. Journal of
605 Geophysical Research. 101**,** 26137-26154.
606 Irwin, P. G. J., et al., 2004. Retrievals of jovian tropospheric phosphine from
607 Cassini/CIRS. Icarus. 172**,** 37-49.
608 Irwin, P. G. J., et al., 1999. Jovian atmospheric studies with the Galileo near infrared
609 mapping spectrometer: An update. Adv. Space Res. 23**,** 1623-1632.
610 Kaye, J. A., Strobel, D. F., 1983. HCN formation on Jupiter - The coupled
611 photochemistry of ammonia and acetylene. Icarus. 54**,** 417-433.
612 Keane, T. C., 1995. The Coupled Photochemistry of Ammonia and Acetylene:
613 Applications to the Atmospheric Chemistry on Jupiter. Ph.D.Thesis. Rensselaer
614 Polytechnic Institute, Troy, New York.
615 Keane, T. C., Yuan, F., Ferris, J. P., 1996. Potential Jupiter atmospheric constituents:
616 Candidates for the mass spectrometer in the Galileo Entry Probe. Icarus. 122**,**
617 205-207.
618 Khare, B. N., Sagan, C., 1973. Red clouds in reducing atmospheres. Icarus. 20**,** 311-321.
619 Lacis, A. A., Oinas, V., 1991. A description of the correlated-k distribution method for
620 modelling nongray gaseous absorption, thermal emission, and multiple scattering
621 in vertically inhomogeneous atmospheres. Journal of Geophysical Research. 96**,**
622 9027-9064.
623 Lara, L.-M., Bézard, B., Griffith, C. A., Lacy, J. H., Owen, T., 1998. High-resolution 10-
624 micronmeter spectroscopy of ammonia and phosphine lines on Jupiter. Icarus.
625 131**,** 317-333.
626 Lewis, J. S., Prinn, R. G., 1970. Jupiter's clouds: Structure and composition. Science.
627 169**,** 472-473.
628 Lindal, G. F., et al., 1981. The atmosphere of Jupiter - an analysis of the Voyager radio
629 occultation measurements. Journal of Geophysical Research. 86**,** 8721-8727.
630 Martonchik, J. V., Orton, G. S., Appleby, J. F., 1984. Optical properties of $NH_3$ ice from
631 the far infrared to the near ultraviolet. Appl. Optics. 23**,** 541-547.
632 Miller, E. A., et al., 1996. The visual and infrared mapping spectrometer for Cassini.
633 Proc. SPIE. 2803**,** 206–220.
634 Molton, P. M., Ponnamperuma, C., 1974. Organic synthesis in a simulated jovian
635 atmosphere. III. Synthesis of aminonitriles. Icarus. 21**,** 166-174.

636 Mordaunt, D. H., Ashfold, M. N. R., Dixon, R. N., Loffler, P., Schneider, L., Welge, K.
637 H., 1998. Near threshold photodissociation of acetylene. J. Chem. Phys. 108**,** 519-
638 526.
639 Moses, J. I., Visscher, C., Keane, T. C., Sperier, A., 2010. On the abundance of non-
640 cometary HCN on Jupiter. Faraday Disc. 147**,** 103-136.
641 Nakayama, T., Watanabe, T., 1964. Absorption and photoionization coefficients of
642 acetylene, propyne, and 1-butene. J. Chem. Phys. 40**,** 558-561.
643 Niemann, H. B., et al., 1998. The composition of the Jovian atmosphere as determined by
644 the Galileo probe mass spectrometer. Journal of Geophysical Research. 103**,**
645 22831-22846.
646 Orton, G. S., 1975. Spatially resolved absolute spectral reflectivity of Jupiter: 3390-8400
647 A. Icarus. 26**,** 159-174.
648 Owen, T., Mason, H. P., 1969. New studies of Jupiter's atmosphere. J. Atmos. Sci. 26**,**
649 870-873.
650 Peek, B. M., 1958. The Planet Jupiter. Faber & Faber, London.
651 Pérez-Hoyos, S., Sánchez-Lavega, A., Hueso, R., García-Melendo, E., Legrarreta, J.,
652 2009. The jovian anticyclone BA III. Aerosol properties and color change. Icarus.
653 203**,** 516-530.
654 Ponnamperuma, C., 1976. The organic chemistry and biology of the atmosphere of the
655 planet Jupiter. Icarus. 29**,** 321-328.
656 Prinn, R. G., 1970. UV radiative transfer and photolysis in Jupiter's atmosphere. Icarus.
657 13**,** 424-436.
658 Prinn, R. G., Lewis, J. S., 1975. Phosphine on Jupiter and implications for the Great Red
659 Spot. Science. 190**,** 274-276.
660 Sada, P. V., Beebe, R. F., Conrath, B. J., 1996. Comparison of the structure and dynamics
661 of Jupiter's Great Red Spot between the Voyager 1 and 2 encounters. Icarus. 119**,**
662 311-335.
663 Sagan, C., Khare, B. N., 1971. Experimental jovian photochemistry: Initial results.
664 Astrophys. J. 168**,** 563-569.
665 Sagan, C., Lippincott, E. R., Dayhoff, M. O., Eck, R. V., 1967. Organic molecules and
666 the coloration of Jupiter. Nature. 213**,** 273-274.
667 Sagan, C., Miller, S. L., 1960. Molecular synthesis in simulated reducing planetary
668 atmospheres (abstract). Astron. J. 65**,** 499.
669 Sill, G. T., 1975 The chemistry of the jovian cloud colors. In: T. Gehrels, (Ed.), Jupiter.
670 Univ. Arizona Press, Tucson, pp. 372-383.
671 Simon-Miller, A. A., Banfield, D., Gierasch, P. J., 2001a. Color and the vertical structure
672 in Jupiter's belts, zones, and weather systems. Icarus. 154**,** 459-474.
673 Simon-Miller, A. A., Banfield, D., Gierasch, P. J., 2001b. An HST study of jovian
674 chromophores. Icarus. 149**,** 94-106.
675 Simon-Miller, A. A., Carlson, R. W., Sanchez-Lavega, A., 2013. An intense red jovian
676 cyclone: Another key fo finding the chromophores. Icarus. Submitted.
677 Simon, A. A., Wong, M. H., Orton, G. S., 2015. First resulfs from the Hubble OPAL
678 program: Jupiter in 2015. Astrophys. J. 812:55.
679 Socrates, G., 2001. Infrared and Raman Characteristic Group Frequencies. Wiley,
680 Chichester.

Strycker, P. D., Chanover, N. J., Simon-Miller, A. A., Banfield, D., Gierasch, P. J., 2011. Jovian chromophore characteristics from multispectral HST images. Icarus. 215**,** 552-583.

Taylor, F. W., Atreya, S., Encrenaz, T., Hunten, D. M., Irwin, P. G. J., Owen, T. C., 2004 The composition of the atmosphere of Jupiter. In: F. Bagenal, T. E. Dowling, W. B. McKinnon, (Eds.), Jupiter. Cambridge University Press, Cambridge, pp. 59-78.

Tokunaga, A. T., Ridgway, S. T., Knacke, R. F., 1980. High spatial and spectral resolution 10-micron observations of Jupiter. Icarus. 44**,** 93-101.

Tomasko, M. G., West, R. A., Castillo, N. D., 1978. Photometry and polarimetry of Jupiter at large phase angles. I - Analysis of imaging data of a prominent belt and a zone from Pioneer 10. Icarus. 33**,** 558-592.

Toon, O. B., Ackerman, T. P., 1981. Algorithms for the calculation of scattering by stratified spheres. Appl. Optics. 20**,** 3657-3660.

Tsukada, M., Oka, T., Shida, S., 1972. Photochemical and radiation-induced reactions of acetylene and hydrogen sulfide mixture. Synthesis of thiophene. Chemistry Lett. 1972**,** 437-440.

Van De Hulst, H. C., 1980. Multiple Light Scattering and Radiative Transfer, Vol. 2. Academic Press, New York.

Visconti, G., 1981. Penetration of solar UV radiation and photodissociation in the Jovian atmosphere. Icarus. 45**,** 638-652.

von Zahn, U., Hunten, D. M., Lehmacher, G., 1998. Helium in Jupiter's atmosphere: Results from the Galileo probe helium interferometer experiment. Journal of Geophysical Research. 103**,** 22815-22830.

West, R. A., Strobel, D. F., Tomasko, M. G., 1986. Clouds, aerosols, and photochemistry in the Jovian atmosphere. Icarus. 65**,** 161-217.

Woeller, F., Ponnamperuma, C., 1969. Organic synthesis in a simulated jovian atmosphere. Icarus. 10**,** 386-392.

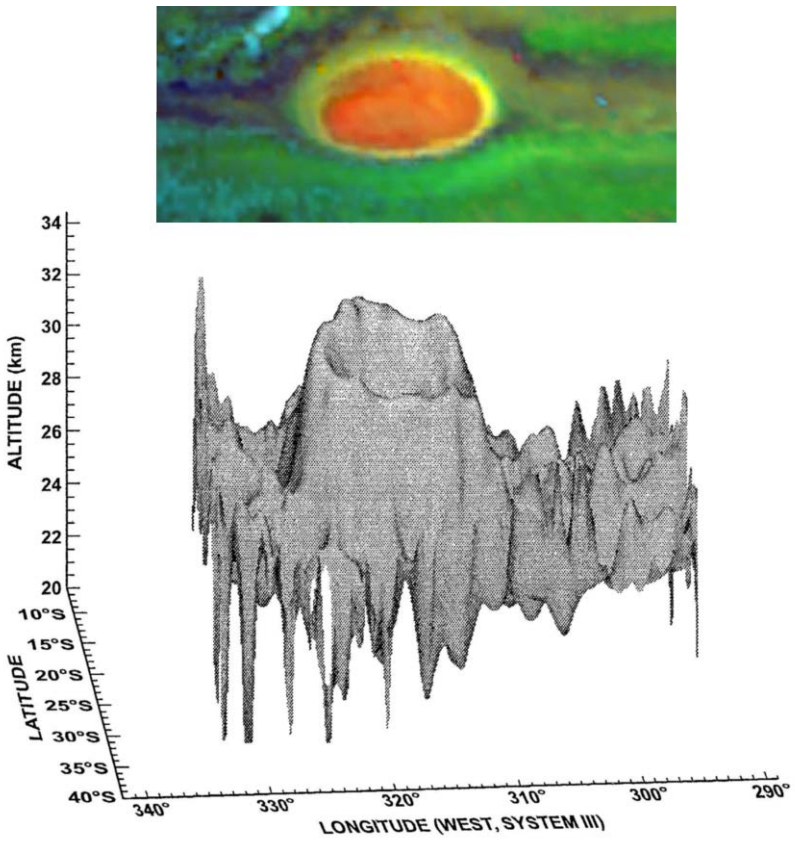


Fig. 1. *Galileo* NIMS false color image of the GRS and corresponding altimetry map. The analysis method to obtain these results is described in the Appendix. In the image, red corresponds to the radiance at 2.06 μm and is in indicator of altitude. Altitudes are relative to the 1-bar level.

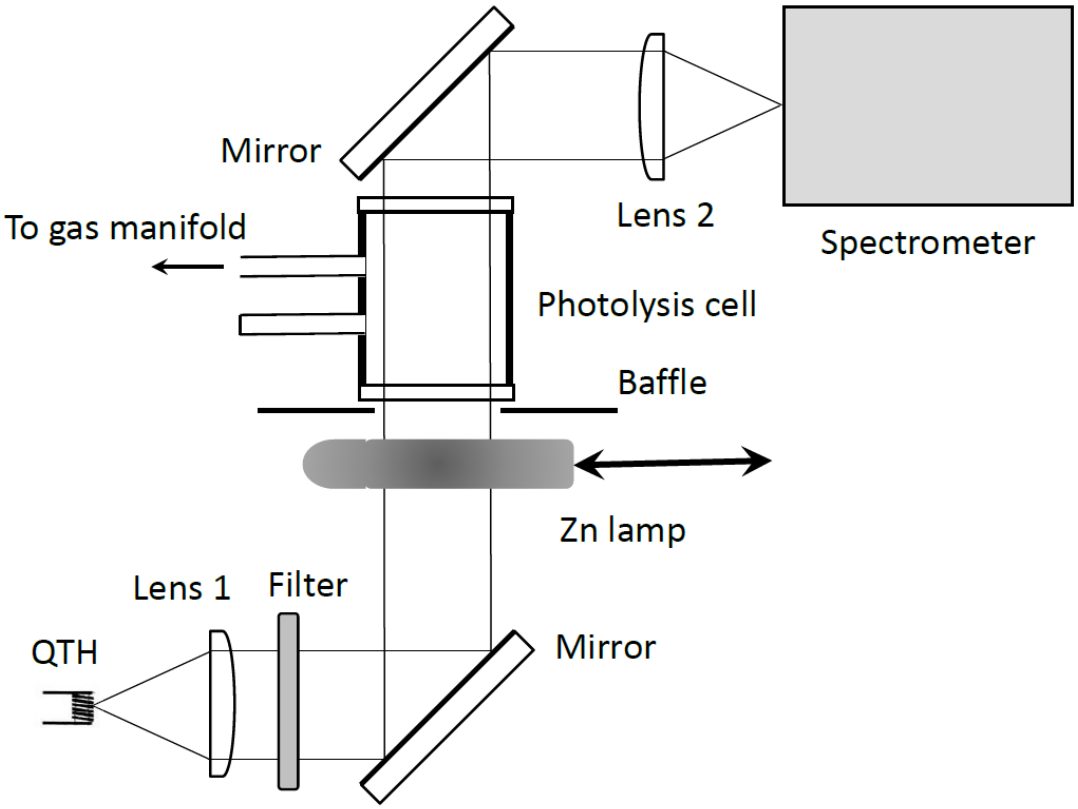


Fig. 2. Experimental arrangement used in the photolysis measurements. The zinc lamp photolyzes $NH_3$ in the gas cell that also contains $C_2H_2$. A resulting yellow-orange film is deposited on the inner surface closest to the lamp. The transmission of the film is measured by removing the Zn lamp and using collimated visible light from a quartz-tungsten-halogen lamp (QTH). The light passing through an order sorting filter, a baffle, the photolysis cell, and then is focused on the entrance slit of a grating spectrometer. The photolysis cell and gas manifold form a closed system but occasionally small samples of gas are withdrawn for analysis.

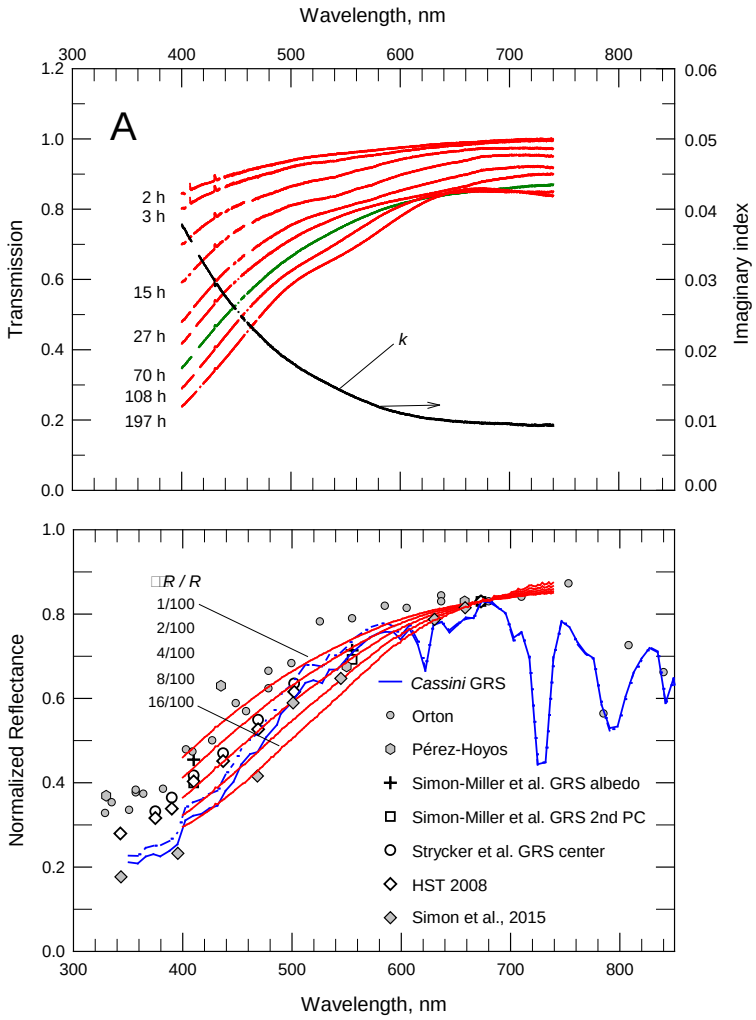


Fig. 3. Laboratory spectra of the photolysis products (upper panel A). Transmission spectra are shown fordifferent average exposure times for Experiment No. 3 (Table 1). The data outages and small glitches correspond to gain-state changes. The 70-hour curve, shown in green, shows minimal effect from channel fringes and was used to derive the chromophore's imaginary index of refraction, shown as the black curve. Panel B shows model calculations (in red) of the GRS reflectivity using the derived index, Mie scattering calculations for spheres with various thicknesses of chromophore coating, and radiative transfer approximations. The calculated reflectivities are consistent with ground-based data obtained by Orton (1975), HST measurements (Simon-Miller et al., 2001b; Pérez-Hoyos et al., 2009; Strycker et al., 2011; Simon et al., 2015) and *Cassini* VIMS spectra. The central pixel of the VIMS observation is shown as the solid blue line; The dashed blue line is the average of central and adjoining eastern and western pixels The *Cassini* and HST 2008 data are discussed in the text and the HST 2008 image is shown in Fig.4B.

Fig. 4. Color comparison of the laboratory-produced chromophore on $SiO_2$ microspheres in transmission (A. at left) with a *Hubble* image (B, at right) using red, green, and blue spectral reflectivities (I/F) images to generate true colors. Note the GRS's dark center and surrounding annulus. The non-uniformity in the laboratory image in A is due to clumping of the $SiO_2$ powder.

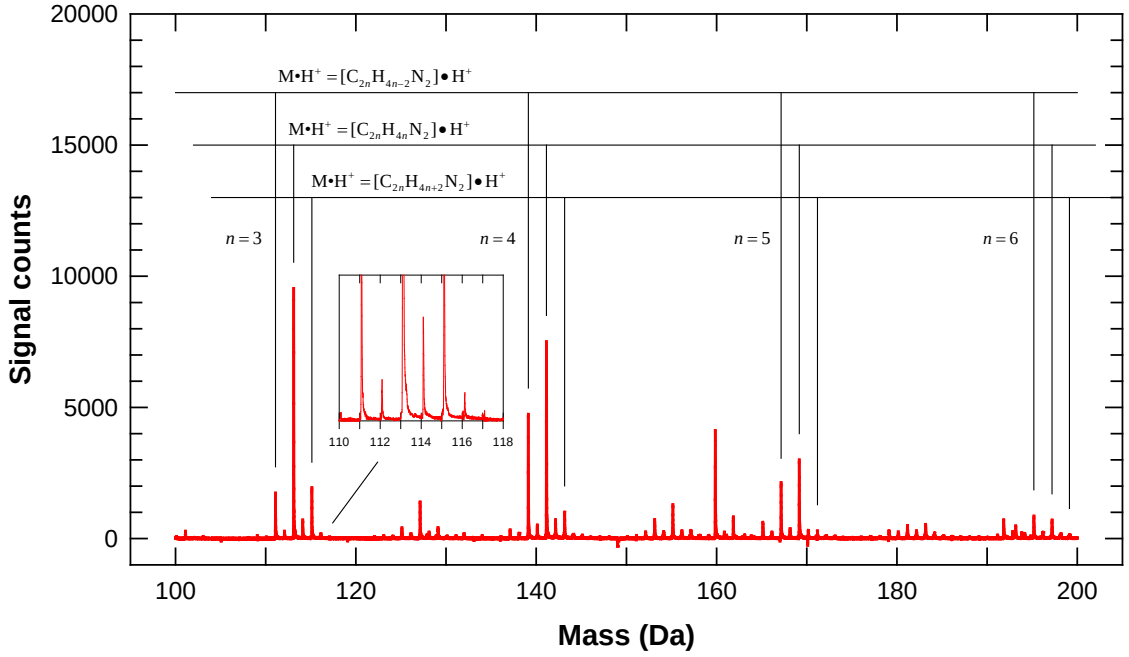


Fig. 5 DART high-resolution mass spectrum of the chromophore-containing deposit produced in Experiment No. 1. Four groups of 3 main members, each containing two N atoms, are shown and are interpreted as combinations of aliphatic azine, azo, and diazo hydrocarbons. The inset shows details of the mass peak profiles and presence of heavier C- and N-isotopes.

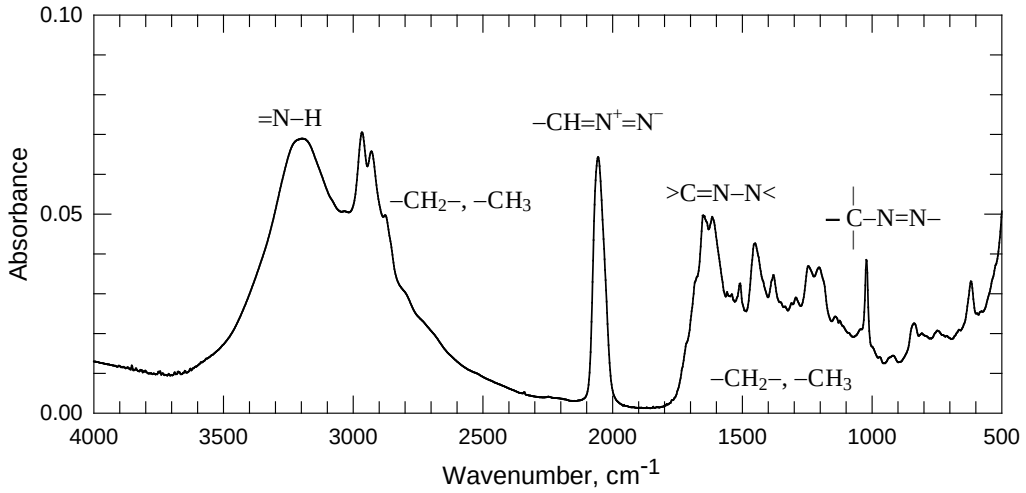


Fig. 6.Infrared spectrum of the experimental chromophore-bearing residue, showing features attributed to the functional groups imine (=N–H), methyl (–$CH_3$), and methylene (–$CH_2$–). The di-nitrogen functional groups are suggested as diazo compounds (RR'C=$N^+$=$N^-$) from the band at 2056 $cm^{-1}$, azines and hydrazones (>C=N–N<) from the C=N stretch transition near 1650 $cm^{-1}$, and azo groups (R–N=N–R') from the C-N stretch band at about 1020 $cm^{-1}$. R represents hydrocarbon radicals.